Enhanced noscapine delivery using estrogen-receptor-targeted nanoparticles for breast cancer therapy

Jitender Madan[a,b], Sushma R. Gundala[a], Yoganjaneyulu Kasetti[c], Prasad V. Bharatam[c], Ritu Aneja[a], Anju Katyal[d] and Upendra K. Jain[b]

Noscapine (Nos), an orally available plant-derived antitussive alkaloid, is in phase II clinical trials for cancer chemotherapy. It has extensively been shown to inhibit tumor growth in nude mice bearing human xenografts of hematopoietic, breast, lung, ovarian, brain, and prostate origin. However, high tumor-suppressive Nos dosages encumber the development of oral controlled-release formulations because of a short biological half-life (<2 h), poor absorption, low aqueous solubility, and extensive first-pass metabolism. Here, we present the design, fabrication, optimization, characterization, and biological evaluation of estrone-conjugated noscapine-loaded gelatin nanoparticles (Nos-ES-GN) for targeting estrogen-receptor-positive breast cancer MCF-7 cells. Gelatin nanoparticles (GN) were a uniformly compact size, stable at physiological pH, and showed a drug entrapment efficiency of 66.1±5.9 and 65.2±5.6% for Nos-GN and Nos-ES-GN, respectively. The secondary structure of gelatin nanocoacervates was predicted using circular dichroism and in-silico molecular modeling. Our data suggest that ethanol-fabricated GN retained the α-helical content of gelatin, whereas acetone favored the formation of random coils. The conjugation of estrone to Nos-GN did not affect the release rate of the drug, and both formulations followed first-order release kinetics with an initial burst, followed by a slow release. The IC_{50} value of Nos-ES-GN was 21.2 μmol/l, which was ~50% lower than the free drug (43.3 μmol/l), suggesting targeted drug delivery. Our cell uptake study carried out in an estrogen-receptor-positive (MCF-7) and negative (MDA-MB-231) cancer cell lines showed greater accumulation of Nos-ES-GN in MCF-7 cells instead of MDA-MB-231 cells. Our data indicated that estrone-conjugated nanoparticles may potentially be used for targeting breast cancer cells. *Anti-Cancer Drugs* 25:704–716 © 2014 Wolters Kluwer Health | Lippincott Williams & Wilkins.

Anti-Cancer Drugs 2014, **25**:704–716

Keywords: breast cancer, cytotoxicity, estrone, gelatin nanoparticles in-silico docking, noscapine

[a]Department of Biology, Georgia State University, Atlanta, Georgia, USA, [b]Department of Pharmaceutics, Chandigarh College of Pharmacy, [c]Department of Medicinal Chemistry, National Institute of Pharmaceutical Education and Research, Mohali, Punjab and [d]Dr. B.R Ambedkar Center for Biomedical Research, University of Delhi, Delhi, India

Correspondence to Jitender Madan, PhD, Department of Pharmaceutics, Chandigarh College of Pharmacy, Mohali, Punjab 140307, India
Tel/fax: +91 172 398 4209; e-mail: jitenderpharmacy@gmail.com

Received 1 November 2013 **Revised form accepted** 6 February 2014

Introduction

Most currently available chemotherapeutic regimens in the clinic are limited by their nonspecificity and nonselectivity for cancer cells that usually manifests as increased toxicity to normal tissues. Owing to serious side effects, anticancer chemotherapeutics are most often administered intermittently at suboptimal doses that result in the eventual failure of therapy, perhaps because of development of drug resistance and subsequent emergence of a more aggressive metastatic disease. Furthermore, reduced intracellular drug accumulation and poor penetration into tumor tissue impede the therapeutic efficacy of many anticancer drugs. Thus, the design and development of therapies that are tumor directed is an area of intense investigation.

Molecularly targeted therapies have recently emerged as an attractive approach to overcome the lack of specificity of conventional chemotherapeutic agents [1]. There is a growing appreciation of receptor-targeted strategies for anticancer drug delivery to achieve superior pharmacokinetic profiles and improved therapeutic indices. Nanoparticles, using both passive and active targeting strategies, can selectively and specifically enhance intracellular drug concentration in cancer cells while sparing normal cells. Furthermore, when targeted ligand-decorated nanoparticles bind to their specific receptors to facilitate cell entry, they are usually enveloped by endosomes by receptor-mediated endocytosis, thereby bypassing the recognition of P-glycoprotein, a major drug efflux pump [2].

Noscapine (Nos) is a microtubule-modulating agent currently in phase II clinical development for the therapy of multiple myeloma. Biopharmaceutically, Nos is a weak base ($pK_a \sim 7.8$) with a mean oral bioavailability of ~31% and a half-life of 1.33 h, which necessitates administration of relatively high doses (300–450 mg/kg body weight) for optimal therapeutic benefits [3–5]. In addition, a short biological half-life (< 2 h), poor absorption, low aqueous solubility, and extensive first-pass metabolism impede the development of an oral controlled-release formulation. Although we recently described the synthesis of supramolecular nanoassemblies to augment aqueous solubility and bioavailability of Nos and brominated Nos, its relatively shorter plasma half-life coupled with

0959-4973 © 2014 Wolters Kluwer Health | Lippincott Williams & Wilkins DOI: 10.1097/CAD.0000000000000098

rapid elimination by first-order kinetics perhaps results in reduced drug accumulation in tumor tissues [5–8].

Estrogen receptors (ERs) are selectively overexpressed up to ~80% in human breast cancers compared with normal breast epithelia [9]. ERs are a group of proteins that are activated by the hormone estrogen. ER is a member of the nuclear hormone family of intracellular receptors, whereas estrogen G protein-coupled receptor GPR30 is a G protein-coupled receptor. ERs are generally designated as cytoplasmic receptors in their unliganded state, but a fraction of the ERs also resides in the nucleus. Once activated by estrogen, the ER is able to translocate into the nucleus and subsequent binding with DNA regulates the activity of different genes [10].

Estrone (ES) binds preferentially to the ER-α receptor found in breast epithelial cells, whereas other ligands such as estriol, raloxifene, and genistein bind to the ER-β receptor. It has been reported that ES sulfate promotes the growth of MCF-7 cells by converting into estradiol by catalytic activity of ES sulfatase and 17β-hydroxysteroid dehydrogenase [11]. MCF-7 cells convert the physiological concentration of ES sulfate into free estradiol, which further stimulates cell growth [12]. However, other analogues of ES such as 2-ethylestrone and 2-ethylestrone-3-*O*-sulfamate induce mitotic arrest and apoptosis in MCF-7 and CAL-51 breast cancer cells, respectively [13]. Coupled with this information, ES hemisuccinate (HS) acts as a ligand to selectively deliver chemotherapeutic agents in breast cancer cells [14]. This offers a unique opportunity to customize ES/estrogen-conjugated drug-loaded nanovesicles for targeting ERs in breast cancer cells [15–17].

In this study, we conjugated gelatin to the activated 3′-HS form of ES to achieve targeted Nos delivery to breast cancer cells. Gelatin, an FDA-approved polymeric coating agent, was used for Nos encapsulation because of its biocompatibility and wider acceptance. Here, we report the design, fabrication, optimization, and characterization of estrone-conjugated noscapine-loaded gelatin nanoparticles (Nos-ES-GN) for targeting ERs and examine their potential for drug delivery *in vitro*.

Materials and methods

Materials

Nos (98% purity), gelatin (type B; bloom strength 225; 100–115 mmol/l of free carboxylic acid/100 g of protein; an isoelectric point of 4.5–5.2; and average molecular weight 40 000–50 000 Da), dimethyl sulfoxide, 3-(4,5-dimethylthiazol-2-yl)-2,5-diphenyltetrazolium bromide (MTT), glutaraldehyde (GLA; 25% aqueous solution), 1-(3-dimethyl-aminopropyl)-3-ethyl-carbodimide hydrochloride, *N*-hydroxysuccinimide, 2,4,6-trinitrobenzenesulfonic acid (TNBS), and ES were from Sigma Aldrich (St. Louis, Missouri, USA). All common reagents and solvents were of the highest analytical grade.

Cells cultures and reagents

Human breast cancer cells (MCF-7 and MDA-MB-231) were maintained in 95% relative humidity and a 5% CO_2 atmosphere at 37°C using Dulbecco's modified Eagle medium (DMEM) supplemented with 5% fetal bovine serum [18].

Synthesis and characterization of ES-modified gelatin using the covalent coupling technique

Synthesis of ES-3′-HS using ES as a template

We have used a previously published method to synthesize the ES-3′-HS from ES [19]. R_f (~0.75) values refer to TLC under ultraviolet (UV) light exposure. Further, the formation of ES-3′-HS from ES was confirmed by measuring the subsequent ^{1}H nuclear magnetic resonance spectroscopy (NMR) and ^{13}C NMR chemical shifts (δ, ppm) because of succinylation.

Conjugation of ES-3′-HS to gelatin

The ES-3′-HS conjugation to gelatin sheets was facilitated by dissolving ES-3′-HS (0.432 g, 1.16 mmol/l) in an equivolume mixture of dioxane and dimethyl formamide. An aqueous mixture was prepared by dissolving *N*-hydroxysuccinimide (0.168 g, 1.45 mmol/l) and 1-(3-dimethyl-aminopropyl)-3-ethyl-carbodimide hydrochloride (0.3 g, 1.45 mmol/l) in 200 µl of distilled water, which was then added to an ES-3′-HS solution. This reaction mixture was vortexed and incubated overnight at 4°C to activate the carboxyl group of ES-3′-HS. A measure of 100 mg of gelatin was then dissolved in 10 ml of distilled water (pH 5.3), followed by the slow addition of the activated steroid, which was further vortexed and incubated overnight at 4°C. The ES–gelatin conjugate was then dialyzed against distilled water and lyophilized [20].

Determination of free amine groups in the conjugate

To ensure successful conjugation of gelatin with ES-3′-HS, the free amine groups in gelatin and ES-conjugated gelatin were determined using the TNBS assay [21].

Preparation and characterization of ES-conjugated gelatin nanoparticles (GN) and gelatin alone bearing Nos

Nos was loaded onto ES-conjugated gelatin (Nos-ES-GN) and gelatin alone (Nos-GN) to compare the kinetics of drug release and cytotoxic activity. Eight formulations of Nos-GN nanoparticles were prepared (Table 2) using the two-step desolvation method [22]. Briefly, 25 ml of a 5% w/v gelatin solution was prepared at room temperature. Gelatin was desolvated by adding 25 ml of acetone or ethanol dropwise and the mixture was left for sedimentation. The supernatant was discarded and the sediment was redissolved in 25 ml of water at varying pH ranging from 2 to 12 with 50 mg of Nos. Acetone or ethanol was again added dropwise to form the GN.

These GN were further cross-linked with GLA (25% aqueous solution), excess of which was neutralized by adding 500 mg of glycine [23]. Purification was performed by centrifugation at 8000*g* and the desolvating agent was removed by slow vaporization over 24 h.

Fluorescein isothiocyanate (FITC) was labeled to an ES-appended formulation using a previously published method [24]. Briefly, ES-GN were dissolved in borate buffer (pH 8.5) at 37°C and labeled as solution A. Separately, FITC solution in borate buffer (pH 8.5) was prepared and labeled as solution B. Both solutions A and B were then mixed and incubated for 3 h at room temperature. The mixture was then dialyzed against distilled water to remove any residual FITC. To determine the labeling efficiencies, the fluorescence intensity of a solution of fluorescein isothiocynate-labeled estrone-conjugated gelatin nanoparticles (FITC-ES-GN) dissolved in PBS (pH 7.4) was measured. The fluorescence intensity (Spectra Fluor; Tecan, Mannedorf, Switzerland; λ_{exe} 485 nm, λ_{emi} 535 nm) was calibrated with standard solutions of 0.005 to 0.013 μg/ml of FITC prepared by diluting 100 μg/ml of methanolic solution of FITC with PBS (pH 7.4). Labeling efficiency was calculated as the percent weight of FITC to weight of the FITC-ES-GN.

$$y = 32750x - 134.7, R^2 = 0.992.$$

Characterization of nanoparticles

Particle size and surface charge analysis

The mean particle size and surface charge (ς) of Nos-GN and Nos-ES-GN were determined using a Zeta-Sizer (Malvern Instruments, Worcestershire, UK).

Encapsulation efficiency and drug-loading capacity

The encapsulation efficiency of all the eight formulations, Nos-GN, Nos-GN$_1$ to Nos-GN$_6$, and Nos-ES-GN (Table 2) was calculated by dispersing the nanoparticles (50 mg) in 50 ml of 0.02 N hydrochloric acid, followed by warming for a few minutes, incubation for 48 h, and centrifugation at 8000*g*. The supernatant was filtered through a 0.2 μm membrane filter and an aliquot of the filtrate was diluted appropriately with the respective solvent system. The concentration of Nos in all the formulations was determined by measuring the optical density at 311.2 nm using a UV–Visible Spectrophotometer (Shimadzu, Kyoto, Japan) [8]. The encapsulation efficiency and drug-loading capacity were calculated using the following formula:

$$\text{Encapsulation efficiency} = \frac{\text{Amount of drug entrapped}}{\text{Amount of drug added}} \times 100.$$

$$\text{Drug loading capacity} = \frac{\text{Amount of drug present}}{\text{Practical yield of nanoparticles}}.$$

Transmission electron microscopy (TEM) and atomic force microscopy (AFM)

Particle shape and morphology of nanoparticles were determined using TEM (Philips Morgagni-268 TEM; Philips Innovation Services, AE Eindhoven, the Netherlands) at a voltage of 80 kV. In addition, AFM was also used to analyze the surface characteristics of Nos-GN and Nos-ES-GN.

Circular dichroism (CD)

The secondary structure of the gelatin nanocoacervate in the solvent phase (ethanol/acetone) was studied using CD spectroscopy, carried out at 25°C with constant nitrogen flushing using a CD instrument (Jasco J-715; Jasco Analytical Services, Easton, Maryland, USA). The far-UV CD spectrum of gelatin was measured from 190 to 250 nm in distilled water at pH ~ 2.5. All measurements were performed in triplicate 10 min after sample preparation with the following instrument settings: 0.5 s, scan speed 200 nm/min, sensitivity 100 millidegrees, and 1 nm spectra band-width. The final concentration of protein used in far-UV CD analysis was 1 mg/ml.

In-silico molecular modeling

Molecular modeling studies were carried out to gain insights into the secondary structure of gelatin nanocoacervate in the solvent phase using Gaussian03 software (Gaussian Inc., Wallingford, Connecticut, USA). Initially, gelatin monomer and dimer models were optimized in the gas phase using semiempirical Austin model 1 (AM1) method [25] implemented in Gaussian03 software. To understand the solvent effect, single point energy calculations were performed on AM1 gas phase-optimized structures at the HF/3–21G* level using the conductor-like polarizable continuum model (CPCM).

In-vitro drug-release kinetics

Dialysis was used to determine the drug-release kinetics of the nanoparticles [26,27]. Briefly, 2 ml of Nos-GN and Nos-ES-GN were placed in dialysis bags (12 kDa; Sigma Aldrich) and dialyzed against 250 ml of PBS (10 mmol/l, pH 4.5) [28] and PBS (10 mmol/l, pH 7.4) maintained at 37°C with a rotation speed of 50 rpm, followed by withdrawal of 5 ml of sample at different time intervals. The samples were further replaced with fresh buffer of the same pH to mimic sink conditions. The Nos concentration in the sample was determined by measuring its optical density using a UV–Visible Spectrophotometer (Shimadzu) at 311.2 nm [8]. The extent of drug release was calculated using a mathematical model based on zero-order or first-order kinetic release of drug from colloidal matrices [26]. The release kinetics was calculated using the following mathematical model [eq. (1)]:

$$\ln\left[\frac{C_1 - Q_m^0}{V_T}\right] = -K_m t + \ln\left[\frac{K_C Q_m^0}{(K_m - K_{CV})} \times V_1 V_2\right]. \quad (1)$$

where C_1 is the concentration of drug in the dialysate (outer solution); $Q_m{}^0$ is the total amount of drug associated with the nanoparticles at time zero; K_m is the first-order release rate constant; K_C is the apparent permeability constant of dialysis tubing; and V_1 and V_2 are the volumes of solution outside and inside the dialysis bag. $V_T = V_1 + V_2$ and $K_{CV} = K_C V_T / V_1 V_2$.

Therapeutic efficacy of Nos-GN and Nos-ES-GN compared with Nos alone: in-vitro studies

In-vitro cytotoxicity assay

The MTT assay [29] was used to evaluate the proliferative capacity of cells treated with various nanoparticle formulations. Briefly, 3×10^3 MCF-7 or MDA-MB-231 cells per well were seeded in a 96-well format. After 24 h of incubation, cells were treated with a gradient concentration of Nos, Nos-GN, and Nos-ES-GN and respective blank formulations. After 72 h of drug incubation, the spent medium was removed and the wells were washed twice with PBS. A final concentration of 5 mg/ml MTT was added to each well and cells were incubated at 37°C in the dark for 4 h. The formazan product was dissolved in 100% dimethyl sulfoxide after removing the medium from each well. The absorbance was measured at 570 nm using a plate reader (Tecan).

In-vitro cellular uptake study: quantitative and qualitative analysis

MCF-7 and MDA-MB-231 cells were plated in separate Petri dishes (35×12 mm) at a density of 3×10^3 cells/Petri plate. Dosing solutions consisted of a freshly prepared FITC-ES-GN formulation [nanoparticle concentration ~6.25–50 μmol/l of Nos encapsulated in Nos-ES-GN in PBS (pH 7.4) diluted with DMEM]. Each cell monolayer was rinsed thrice and preincubated for 1 h with 1 ml of DMEM at 37°C. Uptake was initiated by exchanging the DMEM with 1 ml of specified dosing solution, followed by incubating the cells at 37°C for 5 h. The experiment was terminated by washing the cell monolayer three times with ice-cold PBS (pH ~ 7.4) and lysing the cells with 1 ml of 0.5% Triton X-100. Cell-associated FITC-ES-GN was quantified by analyzing the cell lysate in a fluorimeter (Spectra Fluor, Tecan; λ_{exe} 485 nm, λ_{emi} 535 nm) [30]. The protein content of the cell lysate was measured using the BCA protein assay kit (Pierce Biotechnology Inc., Rockford, Illinois, USA).

After 5 h of incubation, the medium was removed and the plates were washed thrice with sterile PBS. After the final wash, the cells were fixed with 4% paraformaldehyde and individual cover slips were mounted on clean glass slides with fluoromount-G mounting medium (Southern Biotechnology, Birmingham, Alabama, USA). The slides were viewed under a fluorescence microscope (excitation/emission 485/535; Leica Microsystems, Wetzlar, Germany).

Statistical analysis

The results are expressed as the mean ± SD for *n* value 3 or more. Statistical significance was analyzed by one-way and two-way analyses of variance tests. A value of *P* less than 0.05 was considered statistically significant.

Results

Design, preparation, characterization, and optimization of GN

We have designed, developed, and optimized Nos-ES-GN by initially conjugating ES-3′-HS with gelatin sheets, followed by encapsulation of Nos in ES-GN (Scheme 1).

Characterization of ES-conjugated gelatin

Conjugation of ES with gelatin sheets required the synthesis of the ES-3′-HS moiety, followed by the activation of its carbonyl group. Hence, we synthesized ES-3′-HS as the first step in the preparation of ES-conjugated GN, which was characterized by ^{1}H NMR and ^{13}C NMR spectroscopy, as shown in Table 1. Subsequently, the carbonyl group was activated upon incubation with *N*-hydroxysuccinimide and 1-(3-dimethyl-aminopropyl)-3-ethyl-carbodimide hydrochloride in the presence of dioxane and dimethyl formamide. This was followed by conjugation of activated ES-3′-HS to gelatin sheets, resulting in the formation of ES-modified gelatin. The reaction was confirmed by determining the free amine groups that indicate the extent of gelatin modification in ES-conjugated gelatin using a TNBS assay. About 40% of the amine groups in gelatin were found to be modified with ES-3′-HS.

Nos loading onto GN

A series of eight formulations of GN were prepared using a two-step desolvation method by varying various process variables, where gelatin was desolvated in acetone/ethanol to sediment and was then loaded with Nos (Nos-GN). The last member of this series was prepared using the ES-modified gelatin, thus forming Nos-ES-GN (Table 2).

Size characterization of nanoparticles

The size of the nanoparticle determines the effectiveness of drug delivery to the tumor tissue as only appropriately sized nanoparticles can remain in the bloodstream for the required amount of time to selectively deliver the drug to the tumor. An ideal nanoparticle shows compactness in size (> 10 and < 100 nm), that is, it should be large enough to pilot through the leaky blood vessels, but small enough to escape macrophage attack and easily permeate the tumor mass [31]. Hence, we studied the particle morphology, size, and the associated process variables to determine the most effective formulation as observed in Table 2 for further studies.

Scheme 1

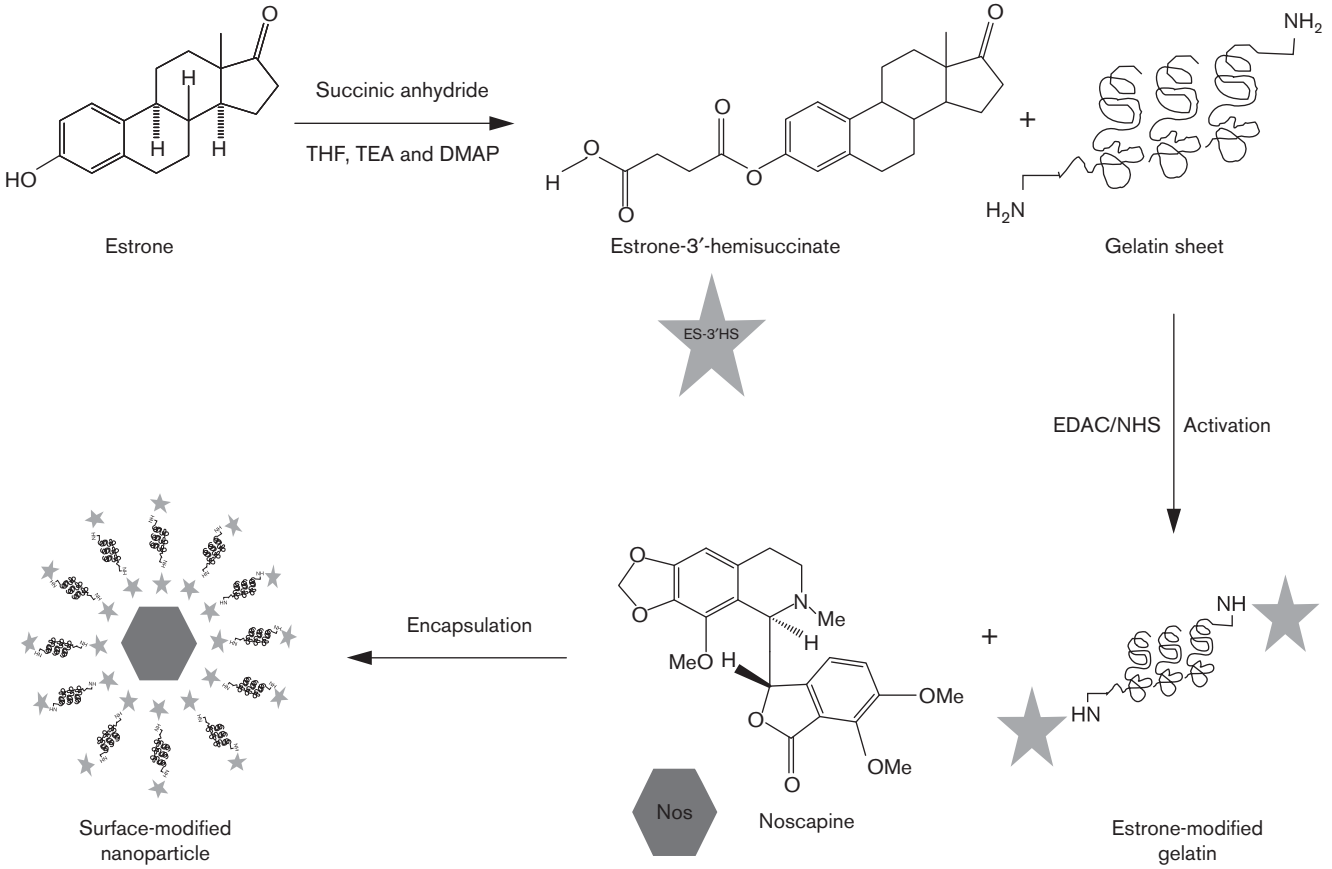

Schematic representation of the preparative steps involved in encapsulation of noscapine (Nos) in estrone-modified gelatin nanoparticles. The estrone-3′-hemisuccinate was conjugated to gelatin sheets to form estrone-modified gelatin. Further, estrone-modified gelatin nanoparticles were constructed to encapsulate noscapine. DMAP, dimethylaminopyrimidine; EDAC, 1-(3-dimethyl-aminopropyl-3-ethyl-carbodiimide hydrochloride; NHS, *N*-hydroxysuccinimide; TEA, triethanolamine; THF, tetrahydrofuran.

Table 1 Characterization of ES and ES-3′-HS by ^{1}H NMR and ^{13}C NMR spectra of ES and ES-3′HS

	^{1}H NMR			^{13}C NMR		
	Position	δ (ppm)	Proton	Position	δ (ppm)	Carbon
ES	4	6.588–6.658	C–H	15	219.73	C=O
	3	2.3–2.39	OH	2, 3	137.9–140.1	C
	16	0.911	CH_3	16	13.82	CH_3
					(77.411	$CDCl_3$
					76.989	
					76.566)	
ES-3′-HS	16	0.907	CH_3	15	219.73	C=O
				4 (A)	178.290	–C=O
	2–3 (A)	3.22	CH_2–CH_2	2, 3	137.9–140.1	C
				16	13.82	CH_3
					(77.41	$CDCl_3$
					76.989	
					76.566)	

A, aliphatic; CD, circular dichroism; ES, estrone; ES-3′-HS, estrone-3′-hemisuccinate; NMR, nuclear magnetic resonance spectroscopy.

Evaluation of particle size on variation of physical parameters

Various physical parameters such as pH, temperature, and surface charge are known to affect the particle size and its dynamics in the bloodstream. We found that the nanoparticle size increased significantly with an increase in the pH of the aqueous gelatin solution from 2.5 to 7.4, as observed in case of Nos-GN, Nos-GN_1, and Nos-GN_2 (130 ± 18 to 180 ± 15 nm) [one-way analysis of variance (ANOVA), $P < 0.05$] (Table 2). When the temperature was varied, with the pH constant, an increase in temperature from 40 to 60°C resulted in an increase in particle size from 130 ± 18 to 287 ± 11 nm as observed for Nos-GN and Nos-GN_4 (two-way ANOVA, $P < 0.0001$) (Table 2). On maintaining pH and temperature constant, an increase in the GLA content from 250 to 500 µl in the formulation did not lead to any considerable change in the nanoparticle size, as observed in the case of Nos-GN (130 ± 18 nm), Nos-GN_5 (125 ± 22 nm), and Nos-GN_6 (127 ± 12 nm) (one-way ANOVA, $P > 0.05$). The maximum noscapine nanoencapsulation efficiency for Nos-GN ($66.1 \pm 5.9\%$) did not appear to be significantly higher than Nos-ES-GN ($65.2 \pm 5.6\%$). However, the ς potential, which is a measure of the surface charge (ς) of nanoparticles indicating the stability in the aqueous phase, decreased for Nos-ES-GN (-33.1 ± 0.8 mV) com-

Table 2 Effect of process parameters on particle size and entrapment efficiency of GN

Samples	pH	Temp (°C)	GLA 25% (μl)	Size (nm)[a]	Polydispersity index[a]	EE (%)[a]	Drug-loading capacity (mg)/10 mg	ς[a] potential (mV)
Nos-GN	2.5	40	250	130±18	0.096±0.026	66.1±5.9	8.26	−40.1±0.5
Nos-GN_1	4.5	40	250	149±21	0.071±0.009	60.8±2.3	–	–
Nos-GN_2	7.4	40	250	180±15	0.099±0.065	35.3±6.2	–	–
Nos-GN_3[b]	2.5	40	250	285±10	0.065±0.010	57.4±4.1	–	–
Nos-GN_4	2.5	60	250	287±11	0.087±0.011	56.1±4.2	–	–
Nos-GN_5	2.5	40	400	125±22	0.110±0.071	55.5±2.9	–	–
Nos-GN_6	2.5	40	500	127±12	0.089±0.067	57.9±3.1	–	–
Nos-ES-GN	2.5	40	250	155±15	0.055±0.074	65.2±5.6	8.35	−33.1±0.8

Acetone was used as the desolvating agent for all the samples.
EE, entrapment efficiency; GLA glutaraldehyde; GN, gelatin; Nos, noscapine; Nos-ES-GN, estrone-conjugated noscapine-loaded gelatin nanoparticles; Temp, temperature.
[a]Values are presented as mean±S.D for $n \geq 3$.
[b]Ethanol was used as a desolvating agent.

Fig. 1

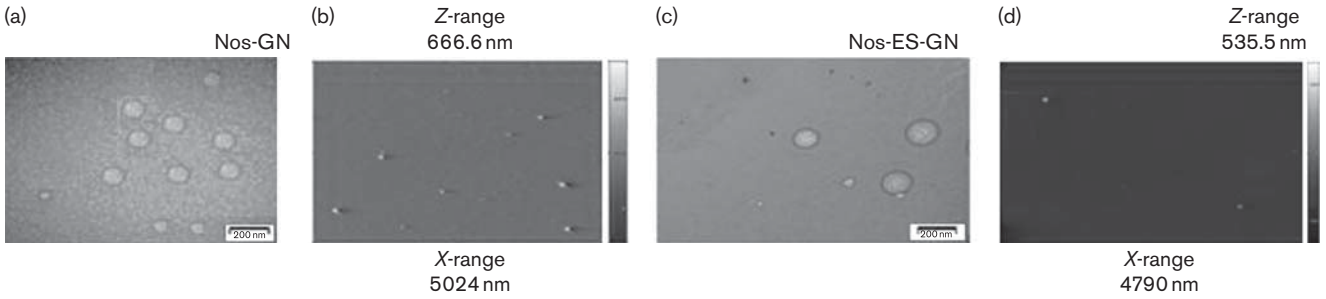

Particle shape and morphology of the nanoparticles were observed by transmission electron microscopy (TEM) and atomic force microscopy (AFM). TEM images of Nos-GN (a) and Nos-ES-GN (b) (scale bar ~ 200 nm). AFM images of Nos-GN (c) and Nos-ES-GN (d). Nos-GN, noscapine-encapsulated gelatin nanoparticles; Nos-ES-GN, estrone-conjugated noscapine-loaded gelatin nanoparticles.

pared with Nos-GN (−40.1 ± 0.5 mV) (two-way ANOVA, $P < 0.05$), measured at the same ionic concentration of PBS. This further confirmed the coating of ES over the surface of GN.

TEM and AFM

We first examined the sizes of nanoparticle formulations using a particle-size analyzer. Subsequently, electron microscopy was used to analyze the surface morphology of optimized formulations. The TEM (Fig. 1a and c) and AFM (Fig. 1b and d) micrographs of lyophilized Nos-GN and Nos-ES-GN suggested that the nanoparticles were smooth and spherical in shape, facilitating their smooth passage through the bloodstream. The TEM micrographs also indicated that centrifugal forces and freeze-drying factors, which are important parameters in nanoparticle preparation, did not affect the nanoparticle texture (Fig. 1a and b).

CD studies and molecular modeling of gelatin nanocoacervates

The process of Nos loading onto GN utilized acetone or ethanol as desolvating agents that influenced the size of nanoparticles (Table 2). Acetone produced smaller nanoparticles (Nos-GN, 130 ± 18 nm) in comparison with ethanol (Nos-GN_3, 285 ± 10 nm), while keeping other variables constant (40°C, 250 μl GLA). To gain further insights into the formation of nanoparticles using acetone or ethanol, we performed CD spectroscopy and in-silico molecular modeling of the gelatin nanocoacervate. Figure 2a shows the CD spectra of an aqueous gelatin solution at pH 7.15 and pH 2.5 with a peak at 200–210 nm and a consistent dip at 230 nm for both solutions. It is recognized that unless an unusual fraction of an aromatic amino acid is present, the optical activity in the region between 190 and 230 nm is governed by the peptide backbone (without any aliphatic side-chain contribution) of proteins, a linear sum of contribution from α-helices, β-turns, and random coils. A similar CD profile, with a peak at 210 nm and a dip at 230 nm, was observed when the aqueous gelatin solution (1 mg/ml, pH 2.5) was titrated gradually with ethanol (Fig. 2b). However, the CD profile of gelatin solution (1 mg/ml, pH 2.5, titrated with acetone; Fig. 2c) indicated the absence of α-helices in gelatin as no dip was observed at 230 nm, a characteristic of the α-helix. This interesting observation led us to carry out in-silico molecular modeling studies to confirm the secondary structure of gelatin nanocoacervate in both the desolvating agents. These studies were carried out using the Gaussian03

Fig. 2

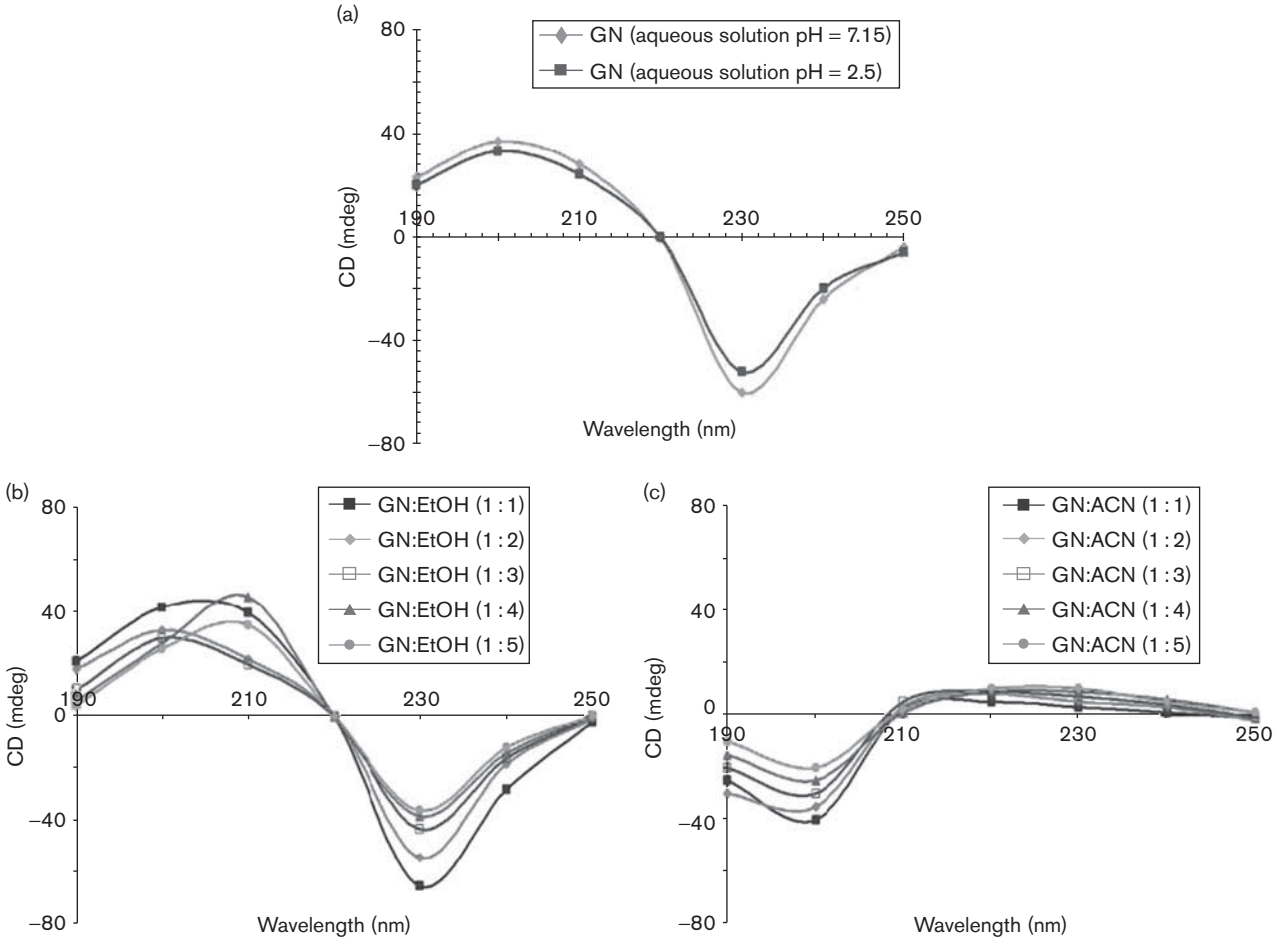

Circular dichroism (CD) curves of aqueous gelatin solution (1 mg/ml) (a), aqueous gelatin solution (1 mg/ml, pH 2.5) titrated with ethanol (EtOH) (b), aqueous gelatin solution (1 mg/ml, pH 2.5) titrated with acetone (ACN) (c). Decrease in pH from its isoelectric point (4.7–5.2) to pH 2.5 retained the secondary structure characteristics of gelatin, whereas titration with ethanol preserves the α-helical contents of gelatin and acetone promotes the formation of random coils. GN, gelatin nanoparticles; mdeg, millidegree.

Table 3 Heat of formation of gelatin monomer and dimers in acetone and ethanol

	Gelatin [heat of formation (AU)]		Stabilization energies (ΔH_f, kcal/mol)	
	Acetone	Ethanol	Gelatin dimers	
Monomer	−2968.1541826	−2968.1582605	Acetone	−17.02
Dimer	−5936.3355026	−5936.3404830	Ethanol	−15.03

Implicit solvent conditions were used on the Austin Model 1 optimized structure. The absolute and relative energy values were reported at the HF/3–21G* level.

software to examine the solvent effect [32]. Initially, gelatin monomer and dimer models were optimized in the gas phase using a semiempirical AM1 method [25]. To understand the solvent effect, single point energy calculations were performed on the optimized structures at the HF/3–21G* level using a CPCM solvation model [33,34]. Binding energy of the gelatin dimer in acetone was −17.02 kcal/mol and the complexation energy was −15.03 kcal/mol in ethanol (Table 3), suggesting the gelatin dimer to be more stable in acetone compared with ethanol (Fig. 3). Hence, these studies predicted that the compactness of the gelatin nanocoacervates may be stronger in acetone than in ethanol.

Drug-release kinetics from GN

In-vitro drug-release kinetics of Nos from GN

One of the factors affecting drug release across the dialysis membrane is the permeability constant [26,27] that was determined by adding a known quantity of drug

Fig. 3

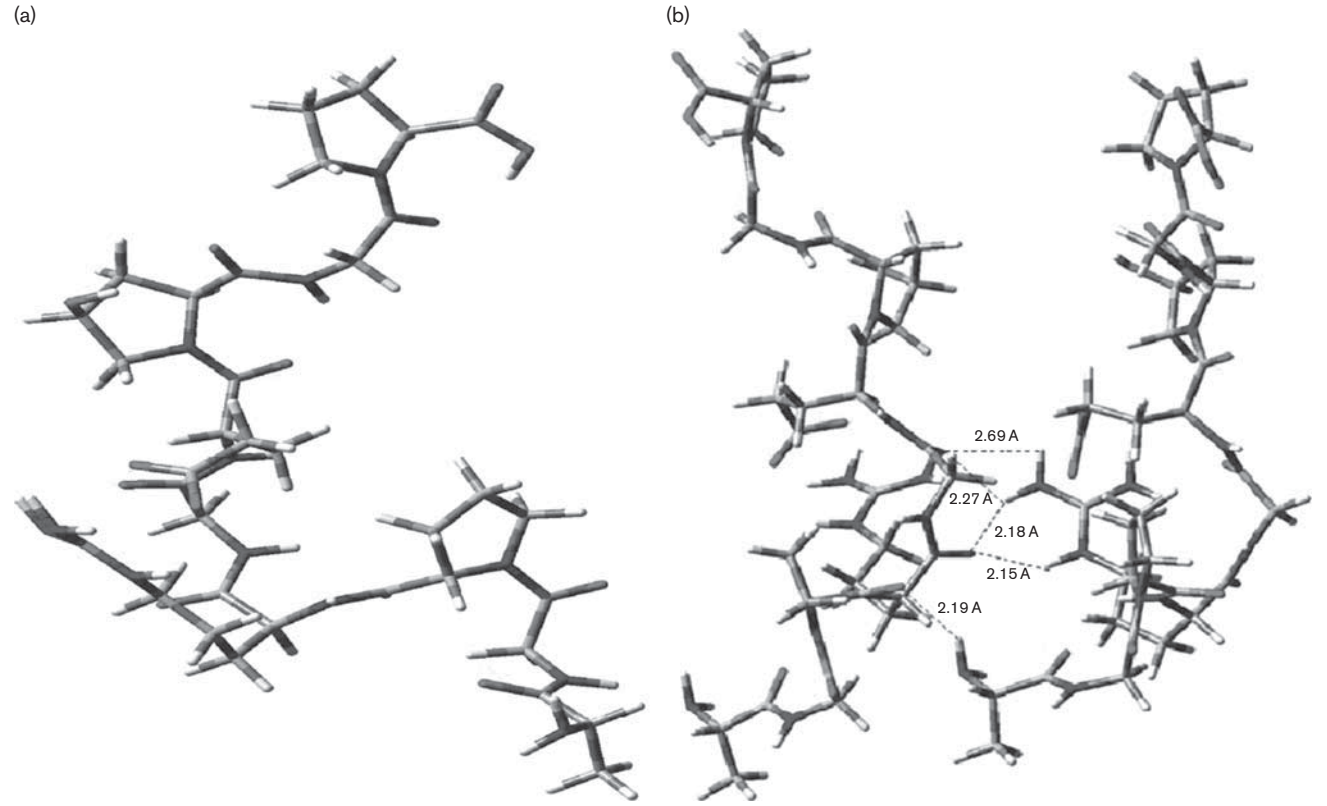

Molecular modeling structures of gelatin monomer (a) and gelatin dimer (b). Gelatin monomer and dimer models were optimized in the Austin model 1 gas phase at the HF/3–21G* level using a conductor-like polarizable continuum model solvent model. The intermolecular hydrogen bond distances were in Å units.

(25 mg/ml Nos) inside the dialysis bag and monitoring the drug concentration in solution outside the bag (C_1) as a function of time. Using the equation for permeability constant ($\mathrm{In}[Q_m{}^0 - C_1(V_1 + V_2)] = \mathrm{In}\ Q_m{}^0 - K_{CV}t$), a plot of $\mathrm{In}[Q_m{}^0 - C_1(V_1 + V_2)]$ versus time yielded the slope ($= K_{CV}$) as 0.0147/h/ml (Fig. 4a). The intercept of the above equation represented the amount of drug present inside the bag (24.95 mg), which was almost equal to the amount loaded (25 mg). This suggested negligible adsorption of Nos on the dialysis membrane. Our data showed that the drug release from Nos-GN and Nos-ES-GN followed first-order release kinetics and showed a biphasic release at pH 4.5 (Fig. 4a) when $\mathrm{In}[C_1 - Q_m{}^0/V_T]$ was plotted against time. Release rate constants for the two phases were determined by the slopes as shown in Table 4. The percent release of drug was calculated following the amount of drug released in both the phases using the rate constant values (Table 4).

Effect of pH on in-vitro release of Nos from GN

We next evaluated the effect of pH on drug release and found that Nos-GN released 47.2 ± 4.5% of Nos in PBS at pH 4.5 in 8 h. However, only 13.2 ± 2.9% of Nos was released at pH 7.4 (Fig. 4b). Similarly, Nos-ES-GN released 40.89 ± 1.8% of Nos in 8 h at pH 4.5 (Fig. 4c). This suggested that enhanced Nos release was found at a pH of 4.5.

Nos-ES-GN showed enhanced efficacy

The cytotoxicity analysis using an in-vitro cell proliferation assay on MCF-7 and MDA-MB-231 cells indicated that the IC_{50} of Nos-ES-GN (21.2 μmol/l) was significantly (one-way ANOVA test, $P < 0.05$) lower than that of Nos-GN (32.1 μmol/l) and Nos alone (43.3 μmol/l) in the MCF-7 cell proliferation assay (Fig. 5). Although there was not much of a significant difference in the IC_{50} values of Nos-GN and Nos-ES-GN, an enhanced cytotoxic effect was observable with the ERs-targeted formulation. In addition, we included MDA-MB-231 breast cancer cells that do not express the ER-receptor as a negative control [35] and found that the IC_{50} value of both formulations (Nos-GN and Nos-ES-GN) was almost similar (36.1 and 33.3 μmol/l, respectively), suggesting that the approximately two-fold lower IC_{50} for Nos-ES-GN in MCF-7 cells might be because of receptor-targeted drug delivery. Blank GN and blank ES-GN had no influence on the cytotoxicity of MCF-7 and MDA-MB-231 cells even at higher concentrations (data not shown) [36,37].

Fig. 4

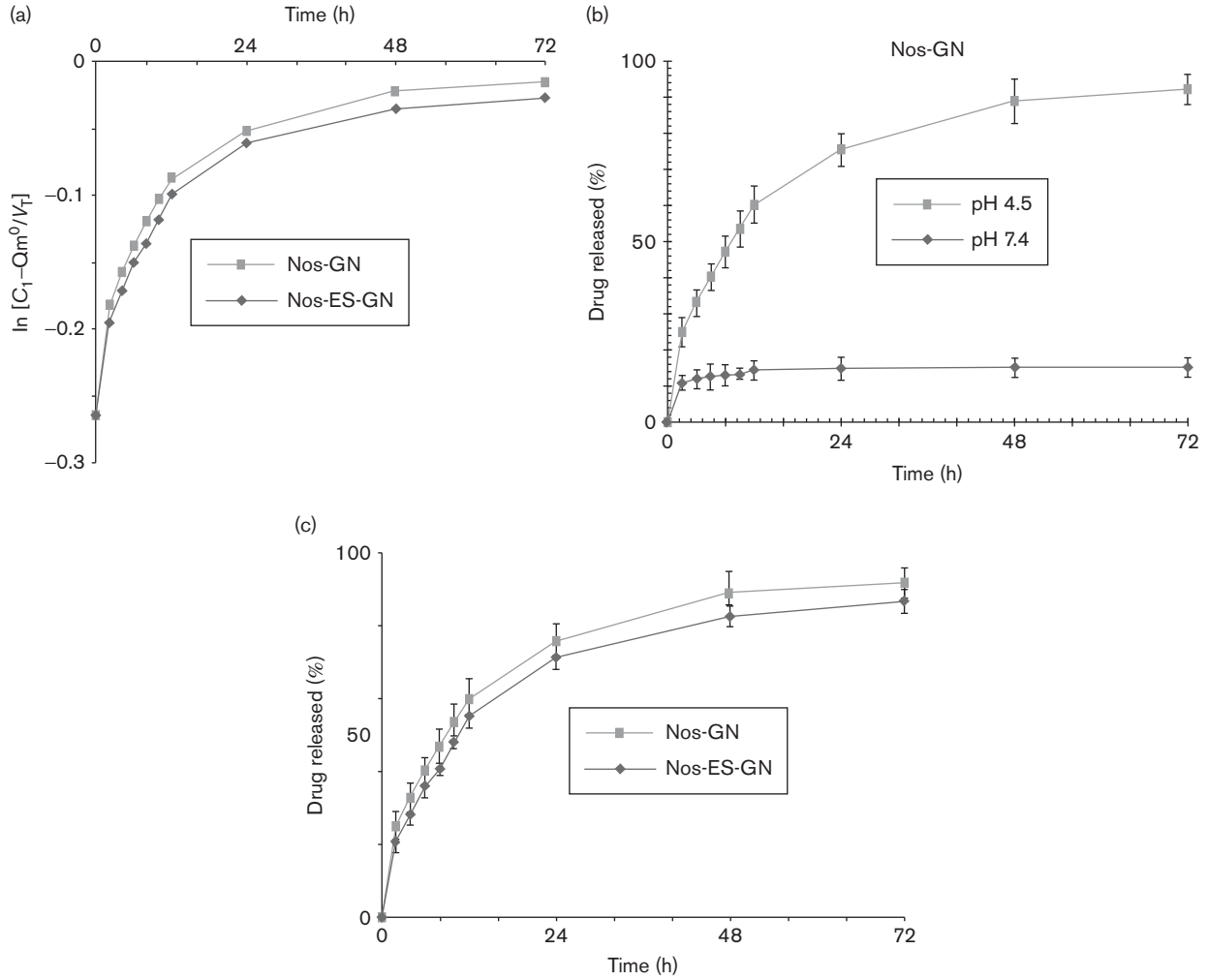

Release kinetics of Nos from Nos-GN and Nos-ES-GN at pH 4.5 was measured as a function of time (a). Drug release was found to follow first-order release kinetics. In-vitro release kinetics of Nos from Nos-GN at pH 4.5 and 7.4 (b). Nos-GN releases 92.1±4.2% of Nos significantly ($P<0.05$) higher than Nos (15.3±2.7%) released at pH 7.4. In-vitro release kinetics of Nos from Nos-GN and Nos-ES-GN at pH 4.5 (c). Nos-GN released 47.2±4.5% of Nos in 8 h ($P<0.05$) higher than Nos released from Nos-ES-GN (40.89±1.8%) at pH 4.5. Values are shown as mean±SD for *n* value 3 or more. Nos, noscapine; Nos-GN, noscapine-encapsulated gelatin nanoparticles; Nos-ES-GN, estrone-conjugated noscapine-loaded gelatin nanoparticles.

Table 4 In-vitro release rate constants for optimized formulations at different phases

Samples	Entrapment efficiency[a]	Release rate constants K_{m1}, K_{m2}, K_m (mg/h)	Initial drug release (%)	Terminal drug release (%)	Total drug release (%)
Nos-GN	66.1±0.9	1.81×10^{-3}, 0.16×10^{-3}, 1.65×10^{-3}	47.2	44.9	92.1
Nos-ES-GN	65.2±0.6	1.60×10^{-3}, 0.17×10^{-3}, 1.43×10^{-3}	40.8	45.8	86.6

K_{m1}, initial rate constant (release of entrapped + free drug); K_{m2}, terminal rate constant (release of entrapped drug); K_m, $K_{m1}-K_{m2}$ (rate constant for the release of free drug).

Nos, noscapine; Nos-ES-GN, estrone-conjugated noscapine-loaded gelatin nanoparticles.

[a]Values are shown as mean±SD for $n \geq 3$.

FITC-ES-GN accumulation in MCF-7 and MDA-MB-231 cells

The quantitative and qualitative cellular accumulation of FITC-ES-GN into MCF-7 and MDA-MB-231 cells was investigated by tracking nanoparticles using fluorimetry (Spectra Fluor; Tecan; λ_{exe} 485 nm, λ_{emi} 535 nm). After incubation of a gradient concentration of FITC-ES-GN with MCF-7 and MDA-MB-231 cells for 5 h, the highest mean fluorescence intensity and cellular accumulation was observed in MCF-7 cells (88.92%), whereas it was less distinctive in MDA-MB-231 cells (33.52%) (Fig. 6a and b).

Fig. 5

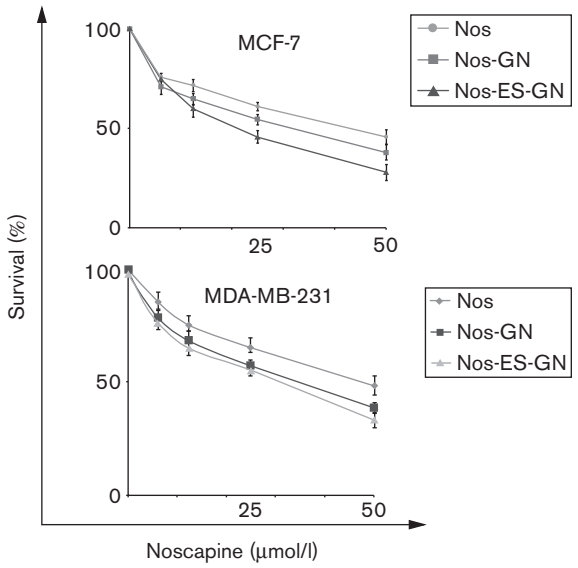

Percent survival profiles of Nos, Nos-GN, and Nos-ES-GN *in vitro* in MCF-7 and MDA-MB-231 breast cancer cells. Nos, noscapine; Nos-ES-GN, estrone-conjugated noscapine-loaded gelatin nanoparticles.

Intracellular tracking of FITC-ES-GN in MCF-7 and MDA-MB-231 cells

The qualitative particle internalization was further examined and visualized by fluorescence microscopy (excitation/emission 485/535; Leica Microsystems). After incubation for 5 h, the intracellular fluorescent spots were observed clearly in cultured MCF-7 cells in the presence of FITC-ES-GN particles. Fluorescence microscopy showed that FITC-ES-GN were distributed homogenously into the cytoplasm of MCF-7 cells in comparison with MDA-MB-231 cells (Fig. 6c).

Discussion

We have shown enhanced drug-release efficacy of Nos-ES-GN targeted to breast cancer MCF-7 cells. These novel nanoparticles were designed, synthesized, and characterized to achieve better targeting of Nos to the ERs selectively overexpressed on breast cancer cells when tumors are hormone responsive [9]. We have optimized formulations taking into consideration the effects of pH, temperature, concentration of GLA, desolvating agents, and entrapment efficiency on nanoparticle size. During the course of experimentation, we found that changes in pH and temperature influenced the nanoparticle size. Essentially, adjustment of pH to 2.5 by adding 0.1 mol/l hydrochloric acid promoted the positive NH_3^+ groups to cross-link with –CHO groups of GLA, facilitating the production of smaller particles. However, larger particles were produced at a pH of 7.4 under similar conditions (Table 2) [38]. Changes in temperature also resulted in varying nanoparticle sizes because of the gelling property of gelatin. In solution, the triple helical structure began to uncoil because of an increase in temperature and thus showed decreased viscosity. In addition, at 40°C, the chains seemed to have sufficiently uncoiled and the addition of a desolvating agent led to a better-controlled precipitation of the macromolecules as compared with a higher temperature (Table 2). CD spectroscopy and molecular modeling studies showed the effect of a desolvating agent on nanoparticle size, wherein ethanol produced larger nanoparticles and acetone resulted in smaller particles (Figs 2 and 3 and Table 2). The process of nanocoacervation induced by the addition of ethanol facilitated the process of inducing chain collapse and interaction of positively charged segments of gelatin with negatively charged ones. Furthermore, ethanol allowed the rupture of hydrogen bonds between water molecules and the polyion. However, water molecules form a hydrogen bond with ethanol molecules and the resultant binary mixture may act as a marginal solvent for gelatin molecules. This perhaps resulted in a reduction in the overall spatial extension of the polyelectrolyte chain, thereby bringing the complementarily charged segments closer. We envisage that this may lead to self-charge neutralization and the formation of gelatin particles in a single chain that were mostly present in the supernatant and the intermolecular segments of complementary charge formed aggregates. As these aggregates may not be fully charge neutralized, they could have attracted other gelatin molecules and thus increased in size (Table 2). Moreover, the dielectric constant of the gelatin aqueous solution also decreased as the volume of ethanol increased, facilitating a stronger electrostatic interaction and hence increase in aggregate size, which drove the system toward coacervation [39]. In contrast, acetone, being a nonpolar solvent, produced smaller particles by decreasing the dielectric constant of water and caused the formation of random coils in the gelatin secondary structure (Figs 2 and 3 and Table 2). This perhaps restricted the interaction of positively charged segments with negatively charged ones and thus did not support the formation of large aggregates, resulting in reduced nanoparticle size. Our molecular modeling studies yielded similar results (Fig. 3) and allow us to propose that favorable hydrogen bonding and electrostatic interaction occurs between two gelatin monomers in acetone, which leads to smaller gelatin coacervates. In the case of ethanol, a relative decrease in favorable hydrogen bonding interactions between two gelatin monomers may have resulted in a loose packing arrangement. A typical structure of gelatin consists of –Ala–Gly–Pro–Arg–Gly–Glu–4Hyp–Gly–Pro–, and AM1 studies [25] under gas phase conditions showed that intermolecular interactions in the gelatin dimer were stabilized by van der Waals interactions in addition to hydrogen bonding (Fig. 3). Our modeling data suggested that the peptide bond oxygen of Pro–Arg may form a hydrogen bond with amino group

Fig. 6

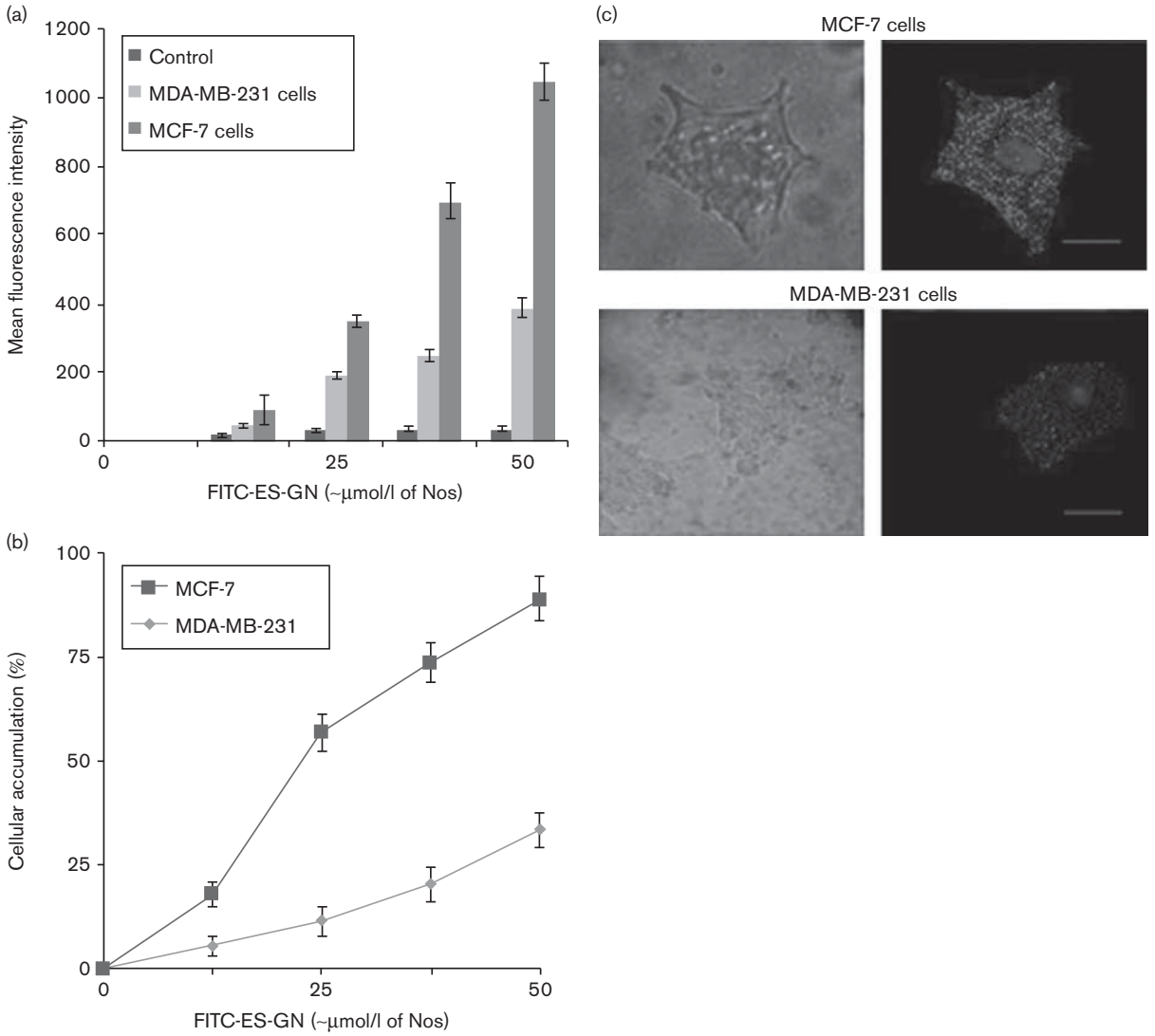

In-vitro cellular uptake of a gradient concentration of FITC-ES-GN incubated with estrogen-receptor-positive (MCF-7) and negative (MDA-MB-231) breast cancer cells line for 5 h (a) mean fluorescence intensity versus gradient concentration of nanoparticles, (b) percent cellular accumulation versus gradient concentration of nanoparticles, (c) representative differential interference contrast and fluorescent images of FITC-labeled ES-GN in MCF-7 and MDA-MB-231 cell lines captured using a fluorescence microscope. FITC-ES-GN appeared in green fluorescence. Cell nucleus was stained with DAPI and appeared in blue (scale bar ~ 20 µm, excitation/emission 485/535; Leica Microsystems). FITC-ES-GN, fluorescein isothiocynate-labeled estrone-conjugated gelatin nanoparticles; Nos, noscapine.

hydrogen of Ala with a distance of 2.19 Å. Similarly, the peptide bond oxygen of Arg–Gly was oriented to form two hydrogen bonds with the H atoms of guanidine at a distance of 2.18 and 2.15 Å. In addition, the peptide bond oxygen of Gly–Glu may form a hydrogen bond with guanidine hydrogen at a distance of 2.27 and 2.69 Å (Fig. 3 and Table 2). Thus, we contemplate that acetone significantly reduces the GN size compared with ethanol. Furthermore, an in-vitro release study at physiological pH to measure the release rate constant suggested that the initial (or first phase) release rate constant was greater than terminal (or second phase), indicating that both surface-adsorbed (free drug) and surface-entrapped drug were released in the first phase, whereas only entrapped drug was released in the second phase (Fig. 4a). Our data also showed that Nos-ES-GN released ~87% of Nos in an acidic environment. The enhanced Nos release from tailored nanoformulations was observed at pH ~ 4.5 in comparison with pH ~ 7.4. This may be attributed to the rigidity of GN at physiological pH, which prevents the swelling of cross-linked gelatin and thus reduces the release rate. However, slightly acidic pH increases the GN size/degree of swelling or the rate of water uptake, which further enhances the release rate. The rate of gelatin swelling is faster in acidic pH because of the ionization of the basic amino acid residues [8,23].

This was favorable as tumors are generally hypoxic and their pH is usually acidic [40] (Fig. 4b). In-vitro cytotoxicity analysis of the three formulations, Nos-GN, Nos-ES-GN, and Nos alone, showed that the IC_{50} of Nos-ES-GN was ~1.5- and ~2-fold lower than that of Nos-GN and Nos alone, respectively, in MCF-7 cells whereas the IC_{50} value of Nos-GN and Nos-ES-GN in MDA-MB-231 cells was almost similar (Fig. 5).

Further, to evaluate whether the surface density of ERs influences the penetration of ES-GN into the cancer cells, cell lines with different expression levels of ERs, MCF-7 and MDA-MB-231 were employed to examine the FITC-ES-GN uptake (Fig. 6a–c). The mechanism that controls ER expression in breast carcinoma elucidated that MCF-7 cells express a 6.5-kb ER mRNA, which actively transcribes the ER gene. However, no ER transcription was detected in MDA-MB-231 cells [41]. Receptor-mediated endocytosis is an essential first step for many antibody-targeted therapies [15–17]. In a similar incubation period, the greater uptake and distribution of FITC-ES-GN in MCF-7 cancer cells may be attributed to the processing of ES-appended formulation by receptor-mediated endocytosis. Therefore, we propose that the receptor-mediated endocytosis pathway would have probably allowed the ES-3′-HS anchored nanoparticles to bind with nuclear ERs, and further processing by ES-ER complexes, instead of favoring the progression of MCF-7 cells [11–14].

Conclusion

We have shown the optimization of Nos-ES-GN for the efficient delivery of Nos into breast cancer cells. Our systematic and methodological investigation of various synthesis parameters governing nanoparticle preparation showed that Nos-GN and Nos-ES-GN can be synthesized with a narrow particle size distribution. In addition, the use of acetone or ethanol as a desolvating agent during the fabrication of nanoparticles was crucial to control the size of nanoparticles to achieve better cellular targeting. Further, in vitro cytotoxicity and the cellular uptake study confirmed that Nos-ES-GN, with greater efficacy compared with Nos alone and Nos-GN, may potentially be used for targeting breast tumor cells. However, more detailed insights into this proof-of-concept study are required to further decode the mechanistic action of an ES-appended formulation including preclinical biodistribution and tumor regression study. The promising in-vitro treatment data of ES appended gelatin nanoformulation bearing Nos deserves further follow-up for preclinical tumor regression study.

Acknowledgements

Conflicts of interest

There are no conflicts of interest.

References

1 Chandra R, Madan J, Singh P, Chandra A, Kumar P, Tomar V, Dass SK. Implications of nanoscale based drug delivery systems in delivery and targeting tubulin binding agent. *Curr Drug Metab* 2012; **13**:1476–1483.

2 Liu CW, Lin WJ. Polymeric nanoparticles conjugate a novel heptapeptide as an epidermal growth factor receptor-active targeting ligand for doxorubicin. *Int J Nanomedicine* 2012; **7**:4749–4767.

3 Olsson B, Bolme P, Dahlstrom B, Marcus C. Excretion of noscapine in human breast milk. *Eur J Clin Pharmacol* 1986; **30**:213–215.

4 Aneja R, Dhiman N, Idnani J, Awasthi A, Arora SK, Chandra R, Joshi HC. Preclinical pharmacokinetics and bioavailability of noscapine, a tubulin-binding anticancer agent. *Cancer Chemother Pharmacol* 2007; **60**:831–839.

5 Madan J, Dhiman N, Parmar VK, Sardana S, Bharatam PV, Aneja R, *et al.* Inclusion complexes of noscapine in beta-cyclodextrin offer better solubility and improved pharmacokinetics. *Cancer Chemother Pharmacol* 2010; **65**:537–548.

6 Madan J, Pandey RS, Jain V, Katare OP, Chandra R, Katyal A. Poly(ethylene)-glycol conjugated solid lipid nanoparticles of noscapine improve biological half-life, brain delivery and efficacy in glioblastoma cells. *Nanomedicine* 2013; **9**:492–503.

7 Madan J, Baruah B, Nagaraju M, Abdalla MO, Yates C, Turner T, *et al.* Molecular cycloencapsulation augments solubility and improves therapeutic index of brominated noscapine in prostate cancer cells. *Mol Pharm* 2012; **9**:1470–1480.

8 Madan J, Dhiman N, Sardana S, Aneja R, Chandra R, Katyal A. Long-circulating poly(ethylene glycol)-grafted gelatin nanoparticles customized for intracellular delivery of noscapine: preparation, *in-vitro* characterization, structure elucidation, pharmacokinetics, and cytotoxicity analyses. *Anticancer Drugs* 2011; **22**:543–555.

9 Dhankhar R, Vyas SP, Jain AK, Arora S, Rath G, Goyal AK. Advances in novel drug delivery strategies for breast cancer therapy. *Artif Cells Blood Substit Immobil Biotechnol* 2010; **38**:230–249.

10 Levin ER. Integration of the extranuclear and nuclear actions of estrogen. *Mol Endocrinol* 2005; **19**:1951–1959.

11 Santner SJ, Ohlsson-Wilhelm B, Santen RJ. Estrone sulfate promotes human breast cancer cell replication and nuclear uptake of estradiol in MCF-7 cell cultures. *Int J Cancer* 1993; **54**:119–124.

12 Billich A, Nussbaumer P, Lehr P. Stimulation of MCF-7 breast cancer cell proliferation by estrone sulfate and dehydroepiandrosterone sulfate: inhibition by novel non-steroidal steroid sulfatase inhibitors. *J Steroid Biochem Mol Biol* 2000; **73**:225–235.

13 MacCarthy-Morrogh L, Townsend PA, Purohit A, Hejaz HAM, Potter BVL, Reed MJ, Packham G. Differential effects of estrone and estrone-3-*O*-sulfamate derivatives on mitotic arrest, apoptosis, and microtubule assembly in human breast cancer cells. *Cancer Res* 2000; **60**:5441–5450.

14 Shcherbakov VM, Devichenskii VM, Vorontsov EA, Kuznetsov SL, Kriukov LN. Synthesis and antiproliferative activity of a novel *N*-acyl derivative of doxorubicin. *Bioorg Khim* 1999; **25**:226–229.

15 Paliwal SR, Paliwal R, Agrawal GP, Vyas SP. Targeted breast cancer nanotherapeutics: options and opportunities with estrogen receptors. *Crit Rev Ther Drug Carrier Syst* 2012; **29**:421–446.

16 Paliwal SR, Paliwal R, Pal HC, Saxena AK, Sharma PR, Gupta PN, *et al.* Estrogen-anchored pH-sensitive liposomes as nanomodule designed for site-specific delivery of doxorubicin in breast cancer therapy. *Mol Pharm* 2012; **9**:176–181.

17 Paliwal SR, Paliwal R, Mishra N, Mehta A, Vyas SP. A novel cancer targeting approach based on estrone anchored stealth liposome for site-specific breast cancer therapy. *Curr Cancer Drug Targets* 2010; **10**:343–353.

18 Ghafouri-Fard S, Abdollahi DZ, Omrani M, Azizi F. shRNA mediated RHOXF1 silencing influences expression of BCL2 but not CASP8 in MCF-7 and MDA-MB-231 cell lines. *Asian Pac J Cancer Prev* 2012; **13**:5865–5869.

19 Li Z, Wang S, Lee NA, Allan RD, Kennedy IR. Development of a solid-phase extraction-enzyme linked immunosorbent assay method for the determination of estrone in water. *Anal Chim Acta* 2004; **503**: 171–177.

20 Basu A, Shrivastav TG, Maitra SK. A direct antigen heterologous enzyme immunoassay for measuring progesterone in serum without using displacer. *Steroids* 2006; **71**:222–230.

21 Fields R. The measurement of amino groups in proteins and peptides. *Biochem J* 1971; **124**:581–590.

22 Azarmi S, Huang Y, Chen H, Mcquarrie S, Abrams D, Roa W, *et al.* Optimization of a two-step desolvation method for preparing gelatin nanoparticles and cell uptake studies in 143B osteosarcoma cancer cells. *J Pharm Pharm Sci* 2006; **9**:124–132.

23 Verma AK, Sachin K, Saxena A, Bohidar HB. Release kinetics from bio-polymeric nanoparticles encapsulating protein synthesis inhibitor, cycloheximide, for possible therapeutic application. *Curr Pharm Biotechnol* 2005; **6**:121–130.

24 Bhavsar MD, Tiwari SB, Amiji MM. Formulation optimization for the nanoparticles-in-microsphere hybrid oral delivery system using factorial design. *J Control Release* 2006; **110**:422–430.

25 Dewar MJS, Zoebisch EG, Healy EF, Stewart JJP. Development and use of quantum mechanics molecular models. 76. AM1: a new general purpose quantum mechanical molecular model. *J Am Chem Soc* 1985; **107**: 3902–3909.

26 Gupta PK, Hung CT, Perrier DG. Quantitation of the release of doxorubicin from colloidal dosage forms using dynamic dialysis. *J Pharm Sci* 1987; **76**:141–145.

27 Illum L, Davis SS. The targeting of drugs parenterally by use of microspheres. *J Parenter Sci Technol* 1982; **36**:242–248.

28 Klimpel D, Cohon MS. pH of intravenous solutions. *N Engl J Med* 1969; **280**:900–901.

29 Mosmann T. Rapid colorimetric assay for cellular growth and survival: application to proliferation and cytotoxicity assays. *J Immunol Methods* 1983; **65**:55–63.

30 Huang M, Ma Z, Khor E, Lim LY. Uptake of FITC-chitosan nanoparticles by A549 cells. *Pharm Res* 2002; **19**:1488–1494.

31 Cho K, Wang X, Nie S, Chen ZG, Shin DM. Therapeutic nanoparticles for drug delivery in cancer. *Clin Cancer Res* 2008; **14**:1310–1316.

32 Frisch MJ, Trucks GW. *Gaussian03 user's reference*. Wallingford, CT: Gaussian Inc.; 2004.

33 Barone V, Cossi M. Quantum calculation of molecular energies and energy gradients in solution by a conductor solvent model. *J Phys Chem A* 1998; **102**:1995–2001.

34 Cossi M, Rega N, Scalmani G, Barone V. Energies, structures, and electronic properties of molecules in solution with the C-PCM solvation model. *J Comput Chem* 2003; **24**:669–681.

35 Kang KS, Morita I, Cruz A, Jeon YJ, Trosko JE, Chang CC. Expression of estrogen receptors in a normal human breast epithelial cell type with luminal and stem cell characteristics and its neoplastically transformed cell lines. *Carcinogenesis* 1997; **18**:251–257.

36 Muvaffak A, Gurhan I, Hasirci N. Prolonged cytotoxic effect of colchicine released from biodegradable microspheres. *J Biomed Mater Res B Appl Biomater* 2004; **71**:295–304.

37 Gupta AK, Gupta M, Yarwood SJ, Curtis AS. Effect of cellular uptake of gelatin nanoparticles on adhesion, morphology and cytoskeleton organization of human fibroblasts. *J Control Release* 2004; **95**: 197–207.

38 Vandervoort J, Ludwig A. Preparation and evaluation of drug-loaded gelatin nanoparticles for topical ophthalmic use. *Eur J Pharm Biopharm* 2004; **57**:251–261.

39 Mohanty B, Bohidar HB. Microscopic structure of gelatin coacervates. *Int J Biol Macromol* 2005; **36**:39–46.

40 Gerweck LE, Seetharaman K. Cellular pH gradient in tumor versus normal tissue: potential exploitation for the treatment of cancer. *Cancer Res* 1996; **56**:1194–1198.

41 Weigel RJ, deConinck EC. Transcriptional control of estrogen receptor in estrogen receptor negative breast carcinoma. *Cancer Res* 1993; **53**:3472–3474.